The Role of His-18 in Amyloid Formation by Human Islet Amyloid Polypeptide†

Andisheh Abedini‡ and Daniel P. Raleigh*,‡,§

Department of Chemistry, State University of New York at Stony Brook, Stony Brook, New York 11794-3400, and Graduate Program in Biochemistry and Structural Biology, Graduate Program in Biophysics, State University of New York at Stony Brook, Stony Brook, New York 11794

Received July 21, 2005; Revised Manuscript Received October 11, 2005

ABSTRACT: The 37-residue islet amyloid polypeptide (IAPP) is the major protein component of the amyloid deposits found in type-II diabetes. IAPP is stored in a relatively low pH environment in the pancreatic secretory granules prior to its release to the extracellular environment. Human IAPP contains a single histidine at position 18. Aggregation of IAPP is considerably faster at a lower pH (4.0 ± 0.3) than at high pH (8.8 ± 0.3), as judged by turbidity and thioflavine-T fluorescence studies. The rate of aggregation at low pH increases drastically in the presence of salt. CD experiments show that the conversion of largely unstructured monomers to β-sheet-rich structures is faster at high pH. TEM studies show that fibrils are formed at both pH values but are more prevalent at pH 8.8 (±0.3). Both the free N terminus of IAPP and His-18 will titrate over the pH range studied. An N-terminal acetylated fragment consisting of residues 8−37 of human IAPP was also studied to isolate contributions from the protonation of His-18. Previous studies have shown that this fragment forms protofibrils that are very similar to those formed by intact IAPP. The effects of varying the protonation state of His-18 in the 8−37 analogue indicate that the rate of aggregation and fibril formation is noticeably faster when His-18 is deprotonated, similar to the wild type. However, the pH-dependent effects are larger for full-length IAPP than for the disulfide-truncated, acetylated analogue. TEM studies indicate differences in the morphology of the deposits formed at high and low pH. These results are discussed in light of recent structural models of IAPP fibrils.

Amyloidoses is a condition belonging to a growing family of degenerative neurological and systemic diseases. Among these diseases, type-II diabetes affects over 150 million people worldwide and has become a leading global health risk in the 21st century (*1*). Type-II diabetes is characterized by chronic insulin resistance and progressive decline in pancreatic β-cell function (*2*, *3*). One of the most common pathological features of type-II diabetes is the deposition of amyloid fibrils in the islets of Langerhans of the pancreas (*4*−*7*). Synthetic amyloid aggregates are toxic to insulin-producing β cells (*8*, *9*), indicating that islet amyloid polypeptide (IAPP)[1] fibril formation in the pancreas may contribute to islet cell dysfunction and death in type-II diabetes mellitus. Human IAPP or amylin, is the major protein component of these amyloid deposits (*10*, *11*). It is cosecreted with insulin into the circulation as a soluble monomer (*12*−*14*). IAPP is stored in the insulin secretory granule, a relatively low pH environment, prior to its release to the extracellular space (*15*). The mature 37-residue IAPP has a Cys-2−Cys-7 disulfide bridge, an amidated C terminus (*10*, *11*), and is involved in the regulation of carbohydrate metabolism (*16*, *17*). Human IAPP contains a single His residue at position 18 whose protonation state should be effected by the change from intragranular to extracellular pH. The sequence of the 37-residue human IAPP polypeptide is shown in Figure 1.

TEM and atomic force microscopy (AFM) studies reveal that the morphological features of synthetic amyloid fibrils derived from human IAPP strongly depend upon the experimental conditions at which they assemble (*18*−*20*). We have previously shown that amyloid formation by short peptides derived from the 10−19 region of human IAPP are strongly influenced by pH (*21*). Above the pK_a of the His-18 residue, the peptide readily aggregates to form amyloid, while aggregation is slower at low pH. Substitution of His-18 to Ala abolishes the pH effects on amyloid formation in this system. His-18 is the only residue in this peptide that titrates over the pH range studied; thus, it should be responsible for the pH-dependent effects. These observations suggest that protonation of His-18 could modulate aggregation by full-length IAPP. Histidine residues also play an important role in amyloid formation by other peptides such as in Alzheimer's Aβ (*22*). Their protonation state can influence β-sheet folding, as well as facilitate zinc binding, which can enhance peptide aggregation (*23*). Earlier studies

† Grant Sponsor: NIH GM54233 to D.P.R.

* To whom correspondence should be addressed: State University of New York at Stony Brook, Stony Brook, NY 11794. Telephone: (631) 632-9547. Fax: (631) 632-7960. E-mail: draleigh@notes.cc.sunysb.edu.

‡ Department of Chemistry.

§ Graduate Program in Biochemistry and Structural Biology, Graduate Program in Biophysics.

[1] Abbreviations: AFM, atomic force microscopy; DMSO, dimethyl sulfoxide; Fmoc, 9-fluorenylmethoxycarbonyl; hIAPP$_{1-37}$, residues 1−37 of human IAPP with an amidated C terminus and free N terminus; hIAPP$_{8-37}$, residues 8−37 of human IAPP with an amidated C terminus and acetylated N terminus; ″HFIP, 1,1,1,3,3,3-hexafluoro-2-propanol; HPLC, high-performance liquid chromatography; IAPP, islet amyloid polypeptide; MALDI−TOF MS, matrix-assisted laser desorption ionization−time-of-flight mass spectrometry; PAL-PEG, 5-(4′-Fmoc-aminomethyl-3′,5-dimethoxyphenol) valeric acid; TEM, transmission electron microscopy; TFA, trifluoroacetic acid; v/v, volume to volume.

10.1021/bi051432v CCC: $30.25
Published on Web 11/12/2005

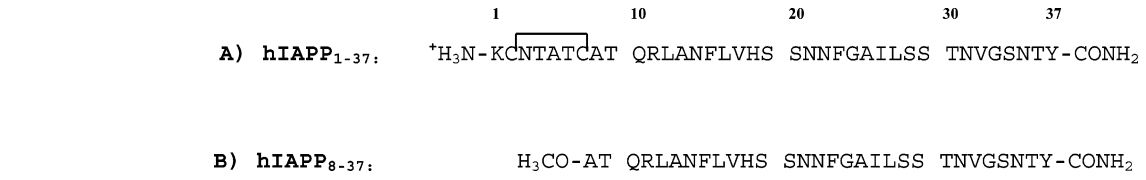

FIGURE 1: Primary sequence of human IAPP. (A) Full-length IAPP ($hIAPP_{1-37}$) with a Cys-2−Cys-7 disulfide bridge and free N terminus. (B) The 8−37 sequence ($hIAPP_{8-37}$) with an acetylated N terminus. All peptides have an amidated C terminus. Residues are numbered according to their position in full-length IAPP.

suggested that the appearance and length of the amyloid fibrils formed by IAPP depend upon pH (*24*). However both His-18 and the N terminus were most likely titrated over the pH range investigated in these experiments, and Tyr-37 may also have been effected at the highest pH values examined; thus, the role of His-18 could not be pinpointed. Here, we examine in more detail the role of His-18 in amyloid formation by human IAPP using the full-length hormone and an analogue with a blocked N terminus. This analogue allows us to isolate the effects of the protonation of His-18 on aggregation. The pH dependence of amyloid formation kinetics is also investigated. Our results are discussed in light of recent structural models of IAPP fibrils.

EXPERIMENTAL PROCEDURES

Peptide Synthesis. Peptides were synthesized on a 0.25 mmol scale with an Applied Biosystems 433A Peptide Synthesizer, using 9-fluornylmethoxycarbonyl (Fmoc) chemistry. Solvents used were ACS-grade. Fmoc-protected pseudoproline (oxazolidine) dipeptide derivatives were purchased from Novabiochem. All other reagents were purchased from Advanced Chemtech, PE Biosystems, Sigma, and Fisher Scientific. Use of a 5-(4′-Fmoc-aminomethyl-3′,5-dimethoxyphenol) valeric acid (PAL-PEG) resin afforded an amidated C terminus. Standard Fmoc reaction cycles were used. The first residue attached to the resin, pseudoproline dipeptide derivatives, all β-branched residues, and all residues directly following a β-branched residue were double-coupled. Peptides were cleaved from the resin using standard trifluoroacetic acid (TFA) methods.

Peptide Purification. To increase solubility, crude peptides were partially dissolved in 20% acetic acid [volume to volume (v/v)], frozen in liquid nitrogen, and lyophilized. This procedure was repeated several times prior to purification. The dry peptides were then redissolved in 35% acetic acid (v/v) and purified via reversed-phase high-performance liquid chromatography (HPLC), using a Vydac C18 preparative column (10 × 250 mm). A two-buffer system was used, utilizing HCl as the ion-pairing agent. Buffer A consisted of H_2O and 0.045% HCl (v/v). Buffer B consisted of 80% acetonitrile, 20% H_2O, and 0.045% HCl (v/v). Purity was checked by HPLC using a Vydac C18 reversed-phase analytical column (4.6 × 250 mm) before each experiment. The identity of the purified peptide was confirmed by matrix-assisted laser desorption ionization−time-of-flight mass spectrometry (MALDI−TOF MS).

Preparation of Peptide Stocks. Biophysical studies utilized peptide samples derived from the same stock solution to ensure comparable conditions in all experiments. Peptide stocks were prepared by adding 1.0 mL of 1,1,1,3,3,3-hexafluoro-2-propanol (HFIP) or dimethyl sulfoxide (DMSO) to dry purified peptide, sonicating at room temperature for 15 s, and lyophilizing. The dry peptide was then redissolved in 1.0 mL of HFIP or DMSO and filtered through a 0.4 μm GHP Acrodisc syringe filter to remove large aggregates. Stock solutions were stored in 2.0 mL polypropylene eppendorf tubes prior to use and frozen at −70 °C between experiments.

Circular Dichroism (CD). All CD experiments were performed at 25 °C on an Aviv 62A DS CD spectrophotometer. For far-UV CD wavelength scans, aliquots of peptide stock were diluted into glycine buffers, for a total volume of 300 μL. The final peptide concentrations for far-UV CD experiments were 0.2 mg/mL in 4% HFIP and 44 mM glycine buffer. Far-UV CD spectra are the average of five repeats in a 0.1 cm quartz cuvette. Spectra were recorded over a range of 190−250 nm, at 1 nm intervals with an averaging time of 3 s. Background spectra were subtracted from collected data. To monitor the development of the β-sheet structure in real time, 12 μL of unfiltered peptide stock solution was diluted in 288 μL of glycine buffer and the CD signal at 218 nm was recorded. The final peptide concentrations for kinetic assays were 0.2 mg/mL in 4% HFIP and 44 mM glycine buffer.

Thioflavin-T-Binding Kinetics. Thioflavin-T-binding assays were used to measure the development of structurally ordered fibrils over time. Fluorescence was measured on a Jobin Yvon Horiba fluorescence spectrophotometer. The excitation wavelength used was 445 nm, and the emission was 485 nm. The excitation and emission slits were set at 5 and 10 nm, respectively. A 1.0 cm cuvette was used. All thioflavin-T kinetic experiments were performed by diluting 68 μL of filtered peptide stock into glycine buffers containing thioflavin-T. Final solution conditions were 44 mM glycine HCl or glycine NaOH and 13.84 μM thioflavin-T at pH 4 (±0.3) and pH 8.8 (±0.3). The total peptide concentration was 0.2 mg/mL in either 4% HFIP or DMSO. Samples used for the ionic strength dependence studies contained 0, 87.5, 175, or 350 mM NaCl. All solutions were stirred during these experiments to maintain homogeneity. As a control, we also monitored the time dependence of the fluorescence of thioflavin-T solutions without the peptide at both pH values. The profiles were flat, indicating that the time-dependent fluorescence observed in the presence of the peptide reflects peptide−dye interactions.

Turbidity Measurements. Solution turbidity was measured as apparent absorbance at 400 nm using a Cary UV−visible spectrophotometer. Experiments were performed by diluting 20 μL of filtered peptide stock into 480 μL of glycine-buffered solution. Final solution conditions were 52 mM glycine HCl or glycine NaOH. The total peptide concentration was 0.2 mg/mL in 4% HFIP. A 1.0 cm quartz cuvette was used.

Transmission Electron Microscopy (TEM). TEM was performed at the University Microscopy Imaging Center at the State University of New York at Stony Brook. TEM samples were prepared by diluting aliquots of unfiltered peptide stock into glycine buffer solutions. The buffer concentration was 44 mM glycine HCl or glycine NaOH. The final peptide concentration was 0.2 mg/mL in 4% HFIP. TEM images were taken within 5 min, 200 min, and 24 h of peptide stock dilution. A total of 4 μL of sample was placed on a carbon-coated 300-mesh copper grid and negatively stained with saturated uranyl acetate.

RESULTS AND DISCUSSION

The Rate of Amyloid Formation by Human IAPP Is Strongly pH-Dependent. Human IAPP has a free N terminus, a histidine at position 18, an arginine at position 11 and a lysine at position 2. These are the only sites that could potentially be positively charged at physiological pH. We examined IAPP fibrillogenesis at pH 4.0 ($\pm$0.3) and pH 8.8 ($\pm$0.3). This pH range was chosen because His-18 will be fully protonated at low pH and fully deprotonated at the highest pH. The pK_a of the N terminus is not known but will certainly be protonated at pH 4.0 and largely deprotonated at pH 8.8. We deliberately avoided using higher pH values to prevent titration of the Lys side chain.

The influence of pH was investigated by CD and thioflavin-T-binding studies at pH 4.0 ($\pm$0.3) and pH 8.8 ($\pm$0.3). Fluorescence-monitored thioflavin-T binding is a standard method for monitoring the development of amyloid fibrils (*25*, *26*). Clear differences in the kinetic profiles of residues 1−37 of human IAPP with an amidated C terminus and free N terminus (hIAPP$_{1-37}$) are observed at the two pH values in both 4% HFIP and DMSO (Figure 2). The fluorescence intensities in DMSO are lower than that in HFIP, which could be a solvent effect or may be due to potential stock-to-stock variability of the peptide concentration. However, the overall trends observed in both systems are consistent and indicate that the time course of thioflavin-T fluorescence is strongly pH-dependent. At pH 4.0 ($\pm$0.3) in 4% HFIP, a slow gain in fluorescence is observed reflecting fibril formation. After 500 min, an apparent plateau of fluorescence is reached, marking the end of the growth phase. In contrast to pH 4.0 ($\pm$0.3), an immediate spike in signal intensity is observed at pH 8.8 ($\pm$0.3) in 4% HFIP. The striking increase in thioflavin-T fluorescence at pH 8.8 ($\pm$0.3) is followed by a steady state after 15 min.

Conformational transitions of hIAPP$_{1-37}$ were probed by time-dependent far-UV CD studies. The size and geometry of the CD cell prevent solution stirring, and aggregation of unstirred filtered samples is very slow under these conditions. Our observation of slower aggregation in the absence of stirring agrees with previous reports that stirring of amyloidogenic peptide solutions increases the rate of fibril formation, possibly by fragmenting long fibrils into smaller ones and increasing the number of active fibril ends for monomers to attach (*27*). Consequently, we examined unfiltered samples. The presence of small preformed oligomers should accelerate the onset of fibril formation, allowing structural transitions to be monitored. Samples were studied at pH 4.0 ($\pm$0.3) and pH 8.8 ($\pm$0.3) at a final peptide concentration of 0.2 mg/mL in 4% HFIP. The increase in

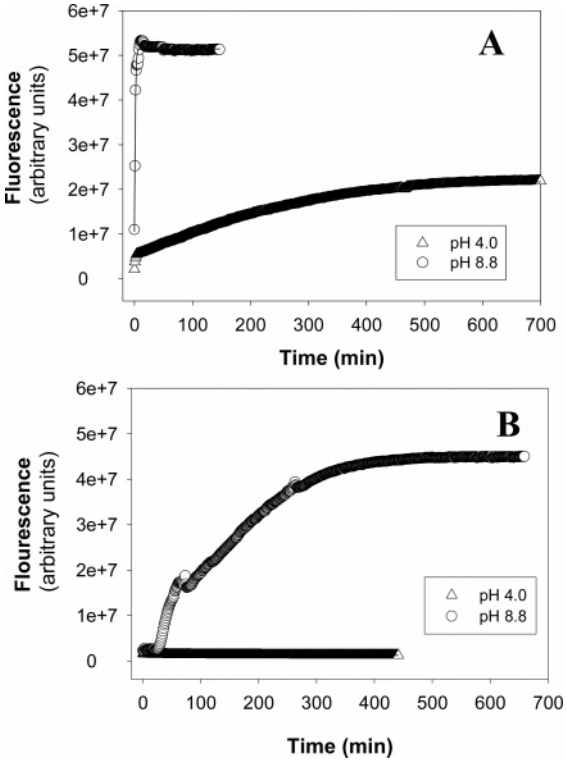

FIGURE 2: Thioflavin-T-binding kinetics of filtered samples of hIAPP$_{1-37}$ monitored at (△) pH 4.0 ($\pm$0.3) and (○) pH 8.8 ($\pm$0.3) in 4% HFIP and 4% DMSO. (A) Kinetic profiles of hIAPP$_{1-37}$ in 4% HFIP. (B) Kinetic profiles of hIAPP$_{1-37}$ in 4% DMSO. The final peptide concentrations for all kinetic assays were approximately 0.2 mg/mL. All samples contained 44 mM glycine buffer. The solid lines represent the fit to a five-parameter sigmoidal curve. These fits were included to aid visualization and have no theoretical significance.

the negative signal at 218 nm indicates an increase in the β structure. Once again, we observe distinct pH effects on the kinetic profiles of hIAPP$_{1-37}$ (Figure 3A). Samples at pH 4.0 ($\pm$0.3) show no relative gain in structure over the 980 min monitored. Wavelength scans taken at the beginning and end of the kinetic reaction further confirm no significant conformational change over the time course (Figure 3B). In contrast, at pH 8.8 ($\pm$0.3), a rapid increase in signal intensity at 218 nm was observed following dilution of the stock solutions. Wavelength scans clearly reveal the structural transition that takes place at this higher pH over time (Figure 3C). Multiple scans averaged over the first 20 min of the kinetic reaction provide evidence for some slight helical structure, which then shifts to a more apparent β-sheet conformation after 450 min.

TEM micrographs were recorded on hIAPP$_{1-37}$ samples prepared at pH 4.0 ($\pm$0.3) and pH 8.8 ($\pm$0.3), exactly as used for the CD studies. Images were recorded after 24 h of incubation at room temperature (Figure 4). Fibrils were observed at both pH values, however with differing extent and morphology. Fibrils at pH 4.0 were much thinner and less prevalent. A dense mat of thicker fibrils were observed at pH 8.8, which largely clumped together on the TEM grid.

The Rate of Fibril Formation by IAPP Is Dependent upon Ionic Strength. The net charge on IAPP is +4 at pH 4 and is between +2 and +3 at pH 8.8, depending upon the exact pK_a of the N terminus. Thus, charge repulsion is expected to disfavor aggregation particularly at low pH. If electrostatic

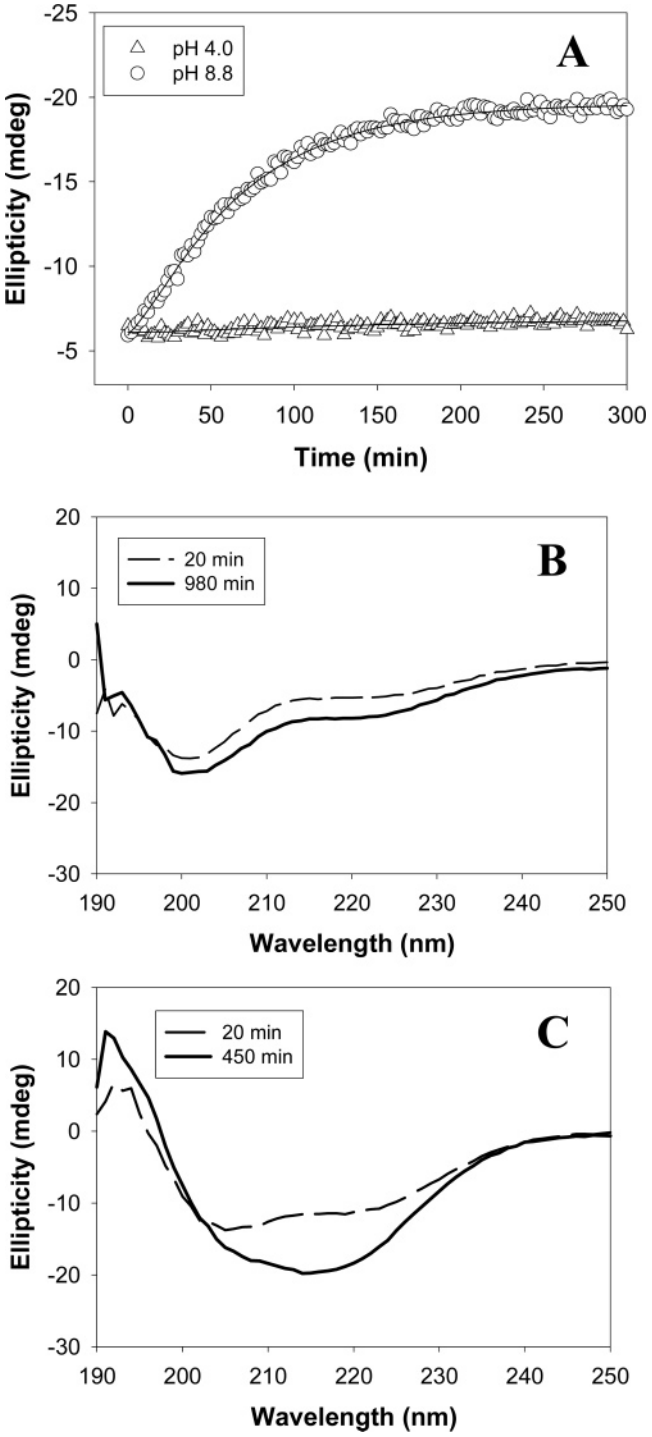

FIGURE 3: (A) Kinetic acquisition of the β-sheet structure by $hIAPP_{1-37}$ at (△) pH 4.0 (±0.3) and (○) pH 8.8 (±0.3) in 4% HFIP. Samples were not filtered or stirred. The CD signal at 218 nm is plotted versus time. (B) Far-UV CD wavelength scans of the pH 4.0 (±0.3) sample recorded at the start of the kinetic experiment (- - -) and the end of the kinetic measurements (—). (C) Far-UV CD wavelength scans of the pH 8.8 (±0.3) sample recorded at the start of the kinetic experiment (- - -) and the end of the kinetic measurements (—). The final peptide concentrations for all kinetic assays were approximately 0.2 mg/mL. The solid lines represent the fit to a five-parameter sigmoidal curve. Curves were included to aid visualization and have no theoretical significance.

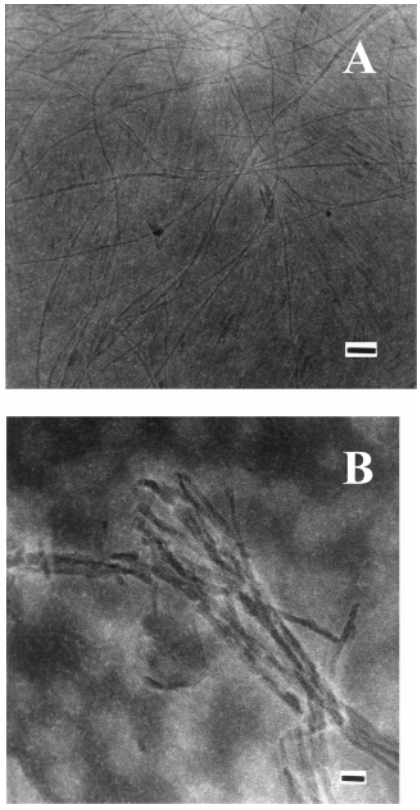

FIGURE 4: TEM micrographs of unfiltered samples of $hIAPP_{1-37}$ at pH 4.0 (±0.3) and pH 8.8 (±0.3). TEM images were recorded 24 h after dilution of the stock solution into buffer. (A) pH 4.0 (±0.3); scale bar represents 50 nm. (B) pH 8.8 (±0.3); scale bar represents 20 nm. The final peptide concentrations for all samples were approximately 0.2 mg/mL in 4% HFIP.

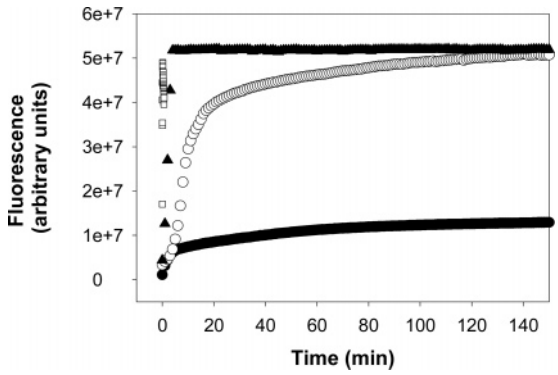

FIGURE 5: Thioflavin-T-binding studies in various amounts of added salt. Samples of $hIAPP_{1-37}$ were filtered and monitored at pH 4.0 (±0.3) in the presence of (●) no salt, (○) 87.5 mM NaCl, (▲) 175 mM NaCl, and (□) 350 mM NaCl. The final peptide concentrations for all samples were approximately 0.2 mg/mL in 4% HFIP. All samples contained 44 mM glycine buffer.

interactions are indeed important, one would expect that the rate of aggregation would increase in the presence of salt. This is exactly what we observe. Thioflavin-T-binding studies were conducted at 0, 87.5, 175, and 350 mM NaCl. Fluorescence measurements indicate that the rate of fibril formation increases monotonically as the NaCl concentration increases. Fibril formation is very slow in the absence of salt at this low pH but increases significantly even with only 87.5 mM added salt. The development of thioflavin-T fluorescence is essentially instantaneous at the highest salt concentration, followed immediately by sample precipitation (Figure 5).

Design of the Peptide Model System To Study the Role of His-18. To evaluate the role of His-18 on the amyloid-forming ability of human IAPP, we synthesized the 8−37

polypeptide sequence with a blocked N terminus and studied it at pH 4.0 (±0.3) and pH 8.8 (±0.3). The pK_a of His-18 in IAPP is not known; however, the peptide is natively unfolded and the pK_a is almost certainly close to standard model compound values. The experimental pH values were chosen to be well below and well above the His pK_a. There are no other residues in the peptide that will titrate over this pH range. The peptide was designated as residues 8−37 of human IAPP (hIAPP$_{8-37}$) and prepared with an amidated C terminus and acetylated N terminus to avoid introducing additional charges (Figure 1). The 8−37 fragment of IAPP is generally considered to be a very good model for amyloid formation by full-length IAPP. The first seven residues of IAPP are thought not to be a part of the ordered core (*20*, 28), and the disulfide-bridged loop between residues 2 and 7 is likely to be incompatible with the formation of ordered cross-β structure. Recent structural models of IAPP fibrils place residues 1−11 outside of the structured core (*29*). A short peptide consisting of residues 1−13 of IAPP does not form amyloid, while short fragments derived from other regions do (*28*). In addition, hIAPP$_{8-37}$ forms protofilaments that are very similar to those formed by hIAPP$_{1-37}$, although the fibril formed by hIAPP$_{1-37}$ contains three protofilaments, while fibrils derived from hIAPP$_{8-37}$ mostly have two (*20*). Because His-18 is the only residue in this sequence that will titrate over the pH range of 4.0−8.8, we can focus on contributions solely at this position and use hIAPP$_{8-37}$ to probe the effects of pH using kinetic and structural methods.

The Protonation State of His-18 Significantly Effects the Rate of Ordered Fibril Formation. The influence of the protonation state of His-18 on the time course of hIAPP$_{8-37}$ fibril formation was investigated by thioflavin-T-binding studies at pH 4.0 (±0.3) and pH 8.8 (±0.3). At pH 4.0, the His-18 side chain is protonated and the total charge on the peptide is +2. At pH 8.8, the His-18 side chain is deprotonated. Experiments were conducted by diluting peptide stock solutions prepared in either HFIP or DMSO into aqueous buffered solution. Two different stock solutions were tested to ensure that the mode of preparation of samples did not significantly affect the results.

As seen with the wild type, thioflavin-T fluorescence is strongly pH-dependent (Figure 6). At pH 4.0 (±0.3), an initial lag phase is observed, followed by a slow gain in fluorescence reflecting fibril formation. After 165 min, an apparent steady-state value of fluorescence is reached. In contrast to pH 4.0 (±0.3), no detectable lag phase is observed at pH 8.8 (±0.3). The rapid sharp increase in thioflavin-T fluorescence at pH 8.8 (±0.3) is followed by visible precipitation of an aggregated peptide. These results are similar to those observed for hIAPP$_{1-37}$ and show that increasing the pH above the pK_a of His-18 significantly increases the rate of ordered fibril formation and decreases solubility. Interestingly, however, the pH-dependent differences in final fluorescence intensity are larger for hIAPP$_{1-37}$ than for hIAPP$_{8-37}$. The final fluorescence in the plateau region reflects the amount of thioflavine bound and hence the amount of ordered material formed and may also reflect the degree of structural order. The fact that the pH-dependent effects are larger for full-length IAPP likely indicates a larger difference in the amount of well-ordered material formed at high and low pH. There are several differences between the peptides studied. Namely, one has a free N terminus, a lysine at position 2 and contains a Cys-2−Cys-7 disulfide, while the other has a blocked N terminus and lacks the disulfide bridge. These differences most likely contribute to the different behavior of the two peptides. Further investigations are in progress to access the relative importance of the disulfide and charged terminus.

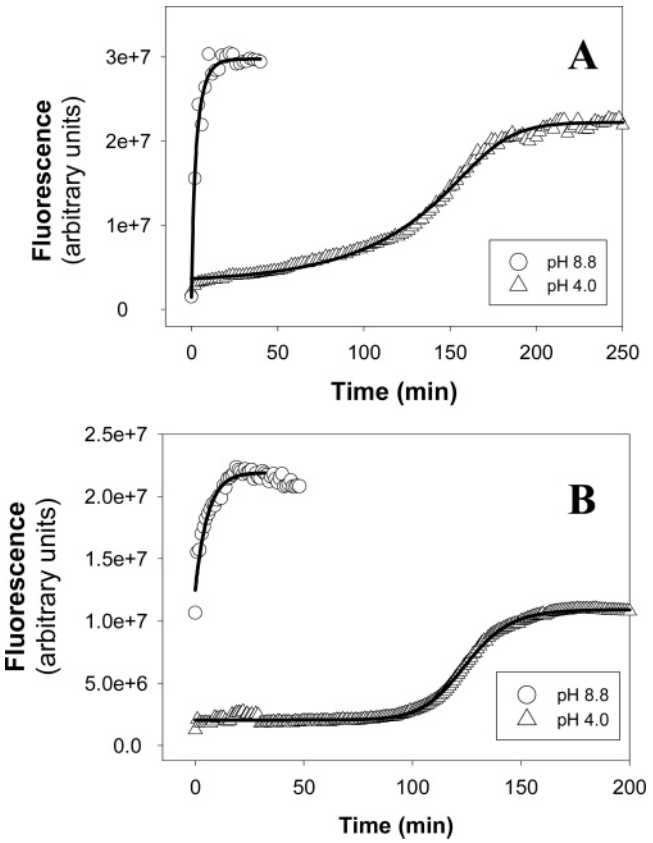

FIGURE 6: Thioflavin-T-binding kinetics of filtered samples of hIAPP$_{8-37}$ monitored at (△) pH 4.0 (±0.3) and (○) pH 8.8 (±0.3) in 4% HFIP and 4% DMSO. (A) Kinetic profiles of hIAPP$_{8-37}$ in 4% HFIP. (B) Kinetic profiles of hIAPP$_{8-37}$ in 4% DMSO. The final peptide concentrations for all kinetic assays were approximately 0.2 mg/mL. All samples contained 44 mM glycine buffer. The solid lines represent the fit to a five-parameter sigmoidal curve. These fits were included to aid visualization and have no theoretical significance.

The time coarse of β-sheet formation by hIAPP$_{8-37}$ was monitored by far-UV CD studies. As seen in the wild-type samples, we observe distinct pH effects on the kinetic profiles of hIAPP$_{8-37}$ (Figure 7A). Measurements at pH 4.0 (±0.3) show a long initial lag phase. In contrast, samples at pH 8.8 (±0.3) exhibit a short lag phase followed by a very sharp increase in the 218 nm signal. Wavelength scans taken at the beginning and end of the two kinetic runs clearly reveal the structural transitions that occur at each pH (parts B and C of Figure 7). In both cases, a shift in minima from 198 nm at time 0 to 218 nm at the end of the time course shows an apparent conversion from a random-coil to β-sheet conformation. The lower signal intensity at pH 8.8 is a result of peptide precipitation.

Turbidity measurements were also preformed at pH 4.0 (±0.3) and pH 8.8 (±0.3) in 4% HFIP (Figure 8). Turbidity reports on the total amount and size of particles in a solution by the resulting scattered light and therefore is not limited to detection of structures with particular conformations. Turbidity can detect less ordered structures that might not

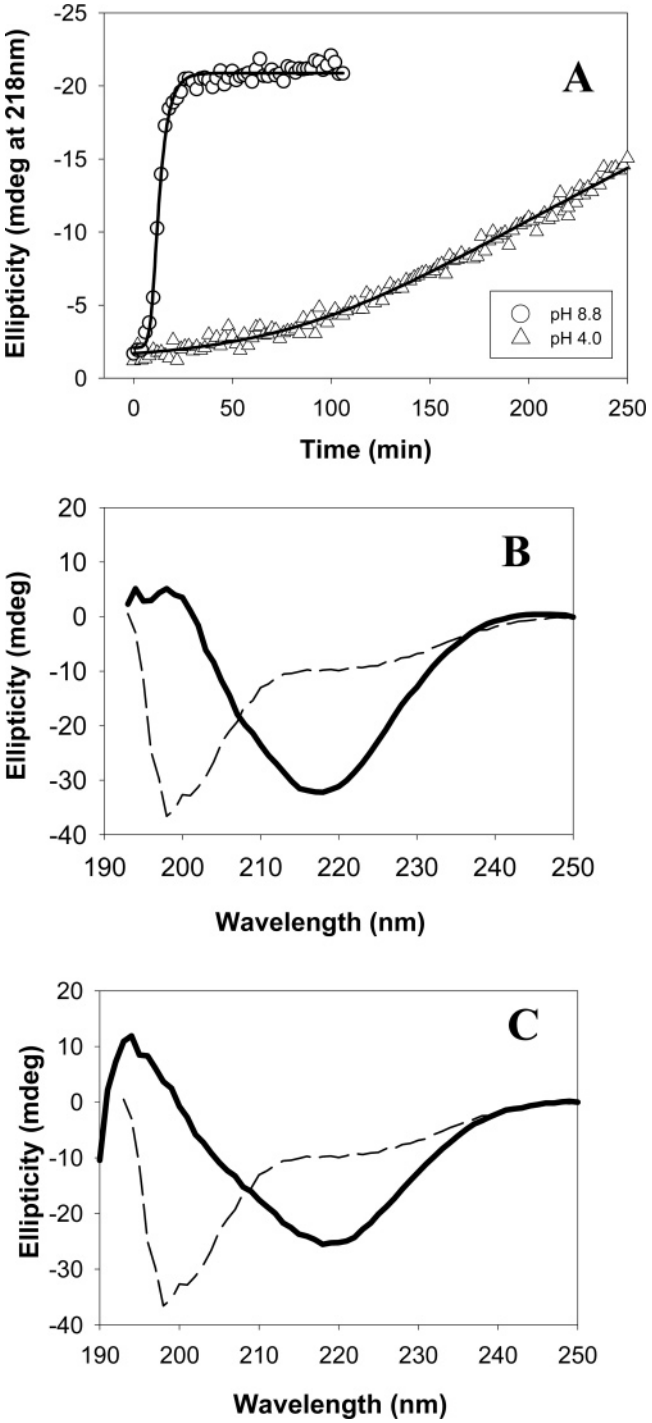

FIGURE 7: (A) Kinetic profiles of the acquisition of the β-sheet structure at (△) pH 4.0 (±0.3) and (○) pH 8.8 (±0.3) in 4% HFIP. Samples were not filtered or stirred. The CD signal at 218 nm is plotted versus time. (B) Far-UV CD wavelength scans of the pH 4.0 (±0.3) sample recorded at the start of the kinetic experiment (- - -) and the end of the kinetic measurements (—). (C) Far-UV CD wavelength scans of the pH 8.8 (±0.3) sample recorded at the start of the kinetic experiment (- - -) and the end of the kinetic measurements (—). The final peptide concentrations for all kinetic assays were approximately 0.2 mg/mL. The solid lines represent the fit to a five-parameter sigmoidal curve. Curves were included to aid visualization and have no theoretical significance.

bind thioflavin-T; thus, the kinetic profiles deduced from turbidity measurements are not required to be coincidental with those generated by thioflavin-T studies. Our turbidity experiments show pH effects similar to those observed with

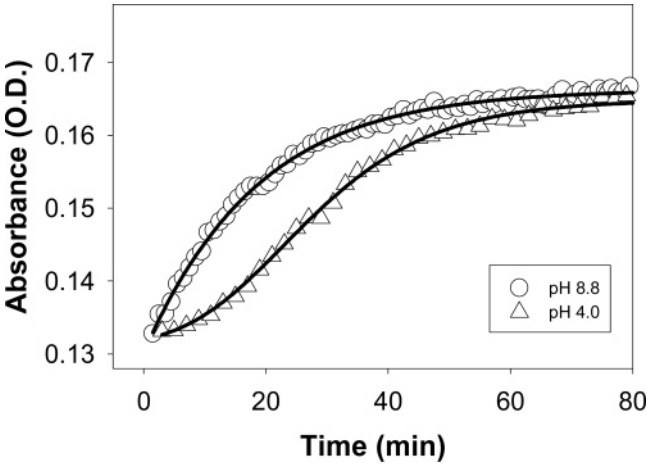

FIGURE 8: Solution turbidity studies of filtered $hIAPP_{8-37}$ monitored at (△) pH 4.0 (±0.3) and (○) pH 8.8 (±0.3) in 4% HFIP. Apparent absorbance at 400 nm is plotted versus time. The final peptide concentrations for all kinetic assays were approximately 0.2 mg/mL. The solid lines represent the fit to a five-parameter sigmoidal curve. These fits were included to aid visualization and have no theoretical significance.

the thioflavin-T experiments. The increase in absorbance is more rapid at pH 8.8 (±0.3), indicating a faster rate of aggregation than for pH 4.0 (±0.3). These data supports our previous observation that deprotonation of the His-18 side chain significantly effects the ease at which $hIAPP_{8-37}$ aggregates. Above the pK_a of His-18, polymerizing aggregates quickly clump together to form higher molecular-weight species that precipitate out of solution.

The Protonation State of His-18 Effects $hIAPP_{8-37}$ Fibril Morphology. TEM studies further confirm that $hIAPP_{8-37}$ fibril assembly rates are strongly influenced by pH and show that fibril morphology is affected as well. TEM samples of unfiltered $hIAPP_{8-37}$ (0.2 mg/mL in 4% HFIP) were prepared at pH 4.0 (±0.3) and pH 8.8 (±0.3), and examined within 5 min, 200 min, and 24 h of preparation (Figure 9). Differences in the morphology of the deposits produced at pH 4.0 (±0.3) and pH 8.8 (±0.3) were evident at all time points. After 5 min of incubation, the pH 8.8 (±0.3) samples readily produced large quantities of clustered protofibrils, while micrographs at pH 4.0 (±0.3) show a mat of amorphous peptide aggregates. After 200 min, the thin protofibrils at pH 8.8 (±0.3) laterally assemble to form thicker, more compact filaments. These fibrillar assemblies increase in length and width after 24 h. TEM samples at pH 4.0 (±0.3) begin to show signs of protofibrils after 200 min of incubation, which are slightly thinner than those produced within 5 min at pH 8.8 (±0.3). After 24 h, these thin protofibrils increase in length but maintain their thin linear character. Similar effects were observed with the $hIAPP_{1-37}$ samples, as previously described.

CONCLUSIONS

Our analysis of $hIAPP_{1-37}$ and $hIAPP_{8-37}$ by thioflavin-T fluorescence, turbidity, CD, and TEM demonstrates that the rate of fibril formation is strongly pH-dependent. More specifically, the ionization state of His-18 significantly effects the rate of assembly and morphology of the aggregates formed. All of the studies show that aggregation/fibril formation is faster at pH 8.8 than 4.0. The slower overall

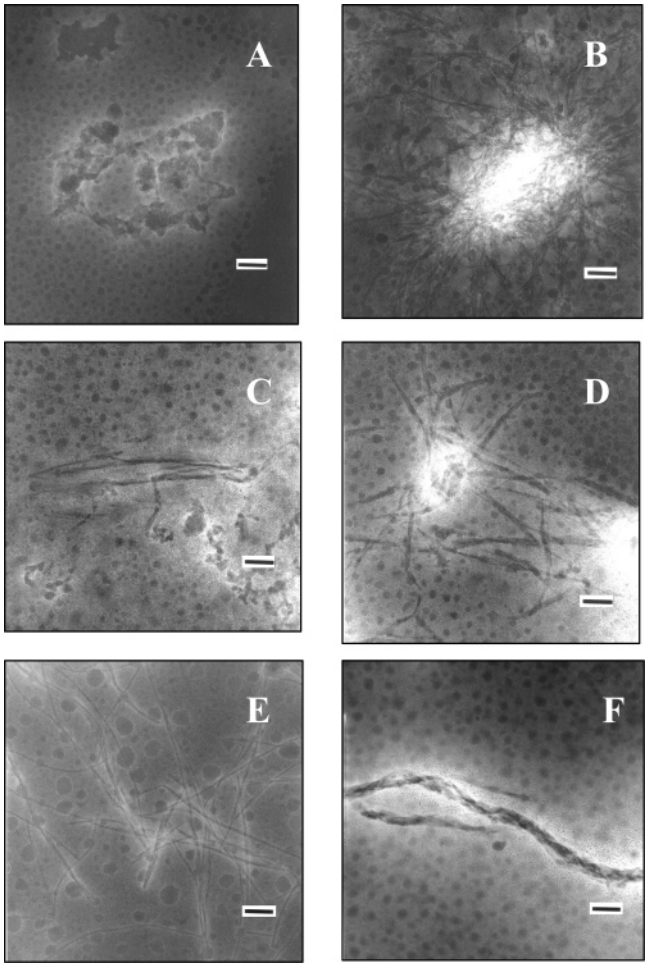

FIGURE 9: TEM micrographs of unfiltered samples of $hIAPP_{8-37}$ at pH 4.0 (±0.3) and pH 8.8 (±0.3). TEM images were recorded at the indicated time after dilution of the stock solution into buffer: (A) 5 min at pH 4.0 (±0.3), (B) 5 min at pH 8.8 (±0.3), (C) 200 min at pH 4.0 (±0.3), (D) 200 min at pH 8.8 (±0.3), (E) 24 h at pH 4.0 (±0.3), and (F) 24 h at pH 8.8 (±0.3). The final peptide concentrations for all samples were approximately 0.2 mg/mL in 4% HFIP. The scale bar represents 100 nm.

rate of fibril assembly when titratable groups are protonated correlates with the higher solubility observed at low pH. The increased charge is expected to increase solubility and should also impede initial oligomerization (*24*, *30*). Mature human IAPP is stored in the β-cell granules of the pancreas at a pH of 5.5 and released into the extracellular compartment, which has a pH of 7.4. The lower pH of the granule should help to reduce irreversible aggregation of IAPP. Factors in addition to pH are also known to play a role in reducing aggregation in the secretory granule (*31*, *32*). Once released, the peptide experiences a pH change that should alter the protonation state of its His-18 residue. As in our *in vitro* experiments, this *in vivo* pH shift could potentially titrate the His-18 side chain and promote the assembly of amyloid. However, because human IAPP does not form amyloid in nondiabetic individuals, factors other than these pH changes must also contribute to amyloid formation (*33*, *34*).

The pH-dependent effects observed here are also consistent with a recently described model of the IAPP fibril. Kajaua et al. have proposed a model in which individual polypeptides form a planar S-shaped structure involving residues 9−37 consisting of three β strands (*29*). The β strands run from Leu-12 to Val-17, Asn-22 to Leu-27, and Thr-30 to Tyr-37. His-18 is located in the turn between strand 1 and 2. The postulated parallel in-register stacking of these basic building blocks would bring His-18 in successive peptides close in space. Such a structure would be expected to be strongly destabilized by charge repulsion when His-18 is protonated.

REFERENCES

1. Zimmet, P., Alberti, K. G. M. M., and Shaw, J. (2001) Global and societal implications of the diabetes epidemic, *Nature 414*, 782−787.
2. Kudva, Y. C., and Butler, P. C. (1997) Insulin secretion in type-2 diabetes mellitus, In *Clinical Research in Diabetes and Obesity*, Vol. 2, Diabetes and Obesity, Humana Press, Totowa, NJ.
3. DeFronzo, R. A. (1988) Lilly Lecture 1987: The triumvirate: Cell, muscle, liver: A collusion responsible for NIDDM, *Diabetes 37*, 667−687.
4. Rocken, C., Linke, R. P., and Saeger, W. (1992) Immunohistology of islet amyloid polypeptide in diabetes mellitus: Semiquantitative studies in a post-mortem series, *Virchows Arch. A Pathol. Anat. Histopathol. 421*, 339−344.
5. Schneider, H. M., Storkel, S., and Will, W. (1980) Das Amyloid der Langerhansschen Inseln und seine Beziehung zum Diabetes mellitus, *Dtsch. Med. Wochenschr. 105*, 1143−1147.
6. Kahn, S. E., Andrikopoulos, S., and Verchere, C. B. (1999) Islet amyloid: A long-recognied but underappreciated pathological feature of type 2 diabetes, *Diabetes 48*, 241−253.
7. Clark, A., Wells, C. A., Buley, I. D., Cruickshank, J. K., Vanhegan, R. I., Matthews, D. R., Cooper, G. J., Holman, R. R., and Turner, R. C. (1988) Islet amyloid, increased A-cells, reduced B-cells, and exocrine fibrosis: Quantitative changes in the pancreas in type 2 diabetes, *Diabetes Res. Clin. Pract. 9*, 151−159.
8. Lorenzo, A., Razzaboni, B., Weir, G., and Yankner, B. (1994) Pancreatic islet cell toxicity of amylin associated with type 2 diabetes mellitus, *Nature 368*, 756−760.
9. Schubert, D., Behl, C., Lesley, R., Brack, A., Dargusch, R., Sagara, Y., and Kimura, H. (1995) Amyloid peptides are toxic via a common oxidative mechanism, *Proc. Natl. Acad. Sci. U.S.A. 92*, 1989−1993.
10. Westermark, P., Wernstedt, C., Wilander, E., Hayden, D. W., O'Brien, T. D., and Johnson, K. H. (1987) Amyloid fibrils in human insulinoma and islets of langerhans of the diabetic cat are derived from a neuropeptide-like protein also present in normal islet cells, *Proc. Natl. Acad. Sci. U.S.A. 84*, 3881−3885.
11. Cooper, G. J. S., Willis, A. C., Clark, A., Turner, R. C., Sim, R. B., and Reid, K. B. M. (1987) Purification and characterization of a peptide from amyloid-rich pancreases of type 2 diabetic patients, *Proc. Natl. Acad. Sci. U.S.A. 84*, 8628−8632.
12. Kahn, S. E., D'Alessio, D. A., Schwartz, M. W., Fujimoto, W. Y., Ensinck, J. W., Taborsky, G. J. J., and Porte, D. J. (1990) Evidence of cosecretion of islet amyloid polypeptide and insulin by β-cells, *Diabetes 39*, 634−638.
13. Sanke, T., T., H., Nakano, Y., Oki, C., Okai, K., Nishimura, S., Kondo, M., and Nanjo, K. (1991) Plasma islet amyloid polypeptide (amylin) levels and their responses to oral glucose in type 2 (non-insulin-dependent) diabetic patients, *Diabetologia 34*, 129−132.
14. Butler, P. C., Chou, J., Carter, W. B., Wang, Y. N., Bu, B. H., Chang, D., Chang, J. K., and Rizza, R. A. (1990) Effects of meal ingestion on plasma amylin concentration in NIDDM and non-diabetic humans, *Diabetes 39*, 752−756.
15. Hutton, J. C. (1989) The insulin secretory granule, *Diabetologia 32*, 271−281.
16. Gebre-Medhin, S., Mulder, H., Pekny, M., Westermark, G., Tornell, J., Westermark, P., Sundler, F., Ahren, B., and Betsholtz, C. (1998) Increased insulin secretion and glucose tolerance in mice lacking islet amyloid polypeptide (amylin), *Biochem. Biophys. Res. Commun. 250*, 271−277.
17. Ahren, B., Oosterwijk, C., Lips, C. J., and Hoppener, J. W. (1998) Transgenic overexpression of human islet amyloid polypeptide inhibits insulin secretion and glucose elimination after gastric glucose gavage in mice, *Diabetologia 41*, 1374−1380.
18. Goldsbury, C., Cooper, G. J. S., Goldie, K. N., Muller, S. A., Saafi, E. L., Gruijters, W. T. M., Misur, M. P., Engel, A., Aebi, U., and Kistler, J. (1997) Polymorphic fibrillar assembly of human amylin, *J. Struct. Biol. 119*, 17−27.

19. Goldsbury, C. S., Kistler, J., Aebi, U., Arvinte, T., and Cooper, G. J. S. (1999) Watching amyloid fibrils grow by time-lapse atomic force microscopy, *J. Mol. Biol. 285*, 33−39.
20. Goldsbury, C., Goldie, K., Pellaud, J., Seelig, J., Frey, P., Muller, S. A., Kistler, J., Cooper, G. J. S., and Aebi, U. (2000) Amyloid fibril formation from full-length and fragments of amylin, *J. Struct. Biol. 130*, 352−362.
21. Tracz, S. M., Abedini, A., Driscoll, M., and Raleigh, D. P. (2004) The role of aromatic interactions in amyloid formation by polypeptides: Analysis of peptides derived from human amylin, *Biochemistry 43*, 15901−15908.
22. Fraser, P. E., McLachlan, D. R., Surewicz, W. K., Mizzen, C. A., Snow, A. D., Nguyen, J. T., and Kirschner, D. A. (1994) Conformation and fibrillogenesis of Alzheimer Aβ peptides with selected substitution of charged residues, *J. Mol. Biol. 244*, 64−73.
23. Emdin, S. O., Dobson, G. G., Cutfield, J. M., and Cutfield, S. M. (1980) Role of zinc in insulin biosynthesis. Some possible zinc−insulin interactions in the pancreatic cell, *Diabetologia 19*, 174−182.
24. Charge, S. B. P., de Koning, E. J. P., and Clark, A. (1995) Effect of pH and insulin on fibrillogenesis of islet amyloid polypeptide *in vitro*, *Biochemistry 34*, 14588−14593.
25. LeVine, H. (1993) Thioflavin-T interaction with synthetic Alzheimer's disease β-amyloid peptides: Detection of amyloid aggregation in solution, *Protein Sci. 2*, 404−410.
26. Kudva, Y. C., Mueske, C., Butler, P. C., and Eberhardt, N. L. (1998) A novel assay *in vitro* of human islet amyloid polypeptide amyloidogenesis and effects of insulin secretory vesicle peptides on amyloid formation, *Biochem. J. 331*, 809−813.
27. Cannon, M. J., Williams, A. D., Wetzel, R., and Myszka, D. G. (2004) Kinetic analysis of β-amyloid fibril elongation, *Anal. Biochem. 328*, 67−75.
28. Jaikaran, E. T. A. S., Higham, C. E., Serpell, L. C., Zurdo, J., Gross, M., Clark, A., and Fraser, P. E. (2001) Identification of a novel human islet amyloid polypeptide β-sheet domain and factors influencing fibrillogenesis, *J. Mol. Biol. 308*, 515−525.
29. Kajava, A. V., Aebi, U., and Steven, A. C. (2005) The parallel superpleated β-structure as a model for amyloid fibrils of human amylin, *J. Mol. Biol. 348*, 247−252.
30. Schmittschmitt, J. P., and Schotz, J. M. (2003) The role of protein stability, solubility, and net charge in amyloid fibril formation, *Protein Sci. 12*, 2378−2378.
31. Westermark, P., Li, Z. C., Westermark, G. T., Leckstrom, A., and Steiner, D. F. (1996) Effects of β-cell granule components on human islet amyloid polypeptide fibril formation, *FEBS Lett. 379*, 203−206.
32. Janciauskiene, S., Eriksson, S., Carlemalm, E., and Ahren, B. (1997) β-Cell granule peptides affect human islet amyloid polypeptide (IAPP) fibril formation *in vitro*, *Biochem. Biophys. Res. Commun. 236*, 580−585.
33. Jaikaran, E. T. A. S., Nilsson, M. R., and Clark, A. (2004) Pancreatic β-cell granule peptides form heteromolecular complexes which inhibit islet amyloid polypeptide fibril formation, *Biochem. J. 377*, 709−716.
34. Larson, J. L., and Miranker, A. D. (2004) The mechanism of insulin action on islet amyloid polypeptide fiber formation, *J. Mol. Biol. 335*, 221−231.

BI051432V